Numerical Simulations of the Epley Maneuver With Clinical Implications

Ismael Arán-Tapia,[1,2,3] Andrés Soto-Varela,[4,5,6] Vicente Pérez-Muñuzuri,[1,3] Sofía Santos-Pérez,[4,5,6] Ismael Arán,[7] and Alberto P. Muñuzuri[1,2]

Objectives: Canalith repositioning procedures to treat benign paroxysmal positional vertigo are often applied following standardized criteria, without considering the possible anatomical singularities of the membranous labyrinth for each individual. As a result, certain patients may become refractory to the treatment due to significant deviations from the ideal membranous labyrinth, that was considered when the maneuvers were designed. This study aims to understand the dynamics of the endolymphatic fluid and otoconia, within the membranous labyrinth geometry, which may contribute to the ineffectiveness of the Epley maneuver. Simultaneously, the study seeks to explore methods to avoid or reduce treatment failure.

Design: We conducted a study on the Epley maneuver using numerical simulations based on a three-dimensional medical image reconstruction of the human left membranous labyrinth. A high-quality micro-computed tomography of a human temporal bone specimen was utilized for the image reconstruction, and a mathematical model for the endolymphatic fluid was developed and coupled with a spherical particle model representing otoconia inside the fluid. This allowed us to measure the position and time of each particle throughout all the steps of the maneuver, using equations that describe the physics behind benign paroxysmal positional vertigo.

Results: Numerical simulations of the standard Epley maneuver applied to this membranous labyrinth model yielded unsatisfactory results, as otoconia do not reach the frontside of the utricle, which in this study is used as the measure of success. The resting times between subsequent steps indicated that longer intervals are required for smaller otoconia. Using different angles of rotation can prevent otoconia from entering the superior semicircular canal or the posterior ampulla. Steps 3, 4, and 5 exhibited a heightened susceptibility to failure, as otoconia could be accidentally displaced into these regions.

Conclusions: We demonstrate that modifying the Epley maneuver based on the numerical results obtained in the membranous labyrinth of the human specimen under study can have a significant effect on the success or failure of the treatment. The use of numerical simulations appears to be a useful tool for future canalith repositioning procedures that aim to personalize the treatment by modifying the rotation planes currently defined as the standard criteria.

Key words: Benign paroxysmal positional vertigo, Canalith repositioning procedure, Epley maneuver, Mathematical modeling, Numerical simulations, Personalized medicine.

Abbreviations: BPPV = benign paroxysmal positional vertigo; CRP = canalith repositioning procedure; EM = Epley maneuver; PTF = probability of treatment failure.

(Ear & Hearing 2024;45;1033–1044)

INTRODUCTION

Vertigo is a very common highly-incapacitating symptom in the general population (Lopez-Escamez et al. 2005). The most frequent cause of vertigo is the benign paroxysmal positional vertigo (BPPV) (Lee & Kim 2010), which has an estimated prevalence of 10 to 140 per 100,000 and a lifetime prevalence of 2.4% (von Brevern et al. 2007; van der Zaag-Loonen et al. 2015).

BPPV is caused by the displacement of otoconia, which under normal conditions are attached to the maculae of the utricle and the saccule. When otoconia dislodge from their usual location in the utricular macula, they become free in the endolymph of the posterior labyrinth and are prone to enter one of the semicircular canals, most commonly the posterior semicircular canal, followed in prevalence by the horizontal and superior canals (van der Zaag-Loonen et al. 2015). Most of the time, otoconia are free in the canal (canalithiasis) and move inside it due to the effect of gravity, when the patient moves his head in a certain direction. This displacement generates a current of endolymph that stimulates the existing sensory cells in the ampulla and consequently produces nystagmus and a subjective sensation of vertigo. Patients with BPPV typically experience recurrent episodes of vertigo that are brief (lasting less than a minute) and are caused by movements of the head, such as lying down, getting up, rolling over in bed, bending over, or looking up.

The treatment for BPPV is based on canalith repositioning procedure (CRP), which aims to redirect otoconia to the vestibule, expelling them from the interior of the semicircular canals. There are specific maneuvers for each canal, but our study focuses on the most used one for the posterior semicircular canal, the Epley maneuver (EM) (Epley 1992). The effectiveness of these maneuvers in resolving the symptoms is very high, with healing rates that exceed 90%. Fortunately, the most common cause of vertigo has an effective and relatively straightforward treatment.

However, a non-negligible number of BPPV patients, estimated by some authors to be around 12.5% of BPPV diagnoses

[1]Group of Non-Linear Physics, Department of Physics, Campus Sur, University of Santiago de Compostela, Santiago de Compostela, Spain; [2]Galician Center for Mathematical Research and Technology, Santiago de Compostela, Spain; [3]Cross-disciplinary Research Center in Environmental Technologies (CRETUS), University of Santiago de Compostela, Santiago de Compostela, Spain; [4]Division of Neurotology, Department of Otorhinolaryngology, Complexo Hospitalario Universitario, Santiago de Compostela, Spain; [5]Department of Surgery and Medical-Surgical Specialities, Universidade de Santiago de Compostela, Santiago de Compostela, Spain; [6]Health Research Institute of Santiago, Santiago de Compostela, Spain; and [7]Department of Otorhinolaryngology, Complexo Hospitalario Universitario de Pontevedra, Pontevedra, Spain.

Supplemental digital content is available for this article. Direct URL citations appear in the printed text and are provided in the HTML and text of this article on the journal's Web site (www.ear-hearing.com).

<zdoi; 10.1097/AUD.0000000000001493>

(Choi et al. 2012), do not experience symptom resolution through the usual maneuvers. Despite receiving a confirmatory diagnosis and undergoing maneuvers multiple times, their symptoms persist. These patients consume a significant amount of healthcare resources, experience prolonged periods of work incapacity, and become a burden for their families. Thus, what initially appears to be a benign and easily solvable disease can become a medical, family, and work problem that persists over time and has no simple solution.

A plausible explanation for the ineffectiveness of the maneuvers in some BPPV patients could stem from individual variations in the anatomical properties of the affected membranous labyrinth. The repositioning maneuvers are designed with the assumption that the membranous labyrinth has an ideal shape, where the angular relationships between the semicircular canals are orthogonal, and the utricle and common crux maintain consistent orientations in relation to these canals. However, it is known that there are differences in the amplitude of these semicircular canal angles between individuals (Della Santina et al. 2005), and there is also certain variability in other regions of the labyrinth (Johnson Chacko et al. 2018). On the basis of this assumption, our hypothesis is that the standard CRP might not be the optimal for the anatomy of a specific patient, and a personalized maneuver that considers the specific vestibular system geometry of the patient could be necessary to enhance the treatment outcome.

Numerical simulation is a noninvasive analytical tool for studying the human vestibular system. This technique enables the investigation of physical parameters that are closely related to those observed experimentally (Wu et al. 2021) and provides an innovative perspective for understanding different vestibular pathologies, such as the Tullio phenomenon (Grieser et al. 2016) or Ménière disease (Rey-Martinez et al. 2020; Senofsky et al. 2023). Several mathematical models have elucidated the behavior of otoconia within the semicircular canals in the context of BPPV (House & Honrubia 2003; Squires et al. 2004; Rajguru et al. 2005; Obrist & Hegemann 2008), providing insights into the mechanisms underlying fatigability (Boselli et al. 2014), and proposing modified maneuvers (Rajguru et al. 2004). Furthermore, in vitro studies on the Semont maneuver have demonstrated the potential to enhance its effectiveness through the incorporation of small variations in the maneuver (Gebhart et al. 2021).

Through a multidisciplinary approach that combines expertise in medicine, physics, and mathematics, our study seeks to investigate the efficacy of the EM and its associated modifications, which are based on the unique anatomical properties of a human membranous labyrinth. Our objective is to assess whether these modifications can enhance the treatment outcomes of BPPV, relieving the functional disability often associated with persistent vertigo, and potentially reducing healthcare costs, particularly in terms of the number of medical consultations.

MATERIALS AND METHODS

Geometric Model

A three-dimensional medical image reconstruction of a left membranous labyrinth was used (Fig. 1). It corresponds to a "post-mortem" human specimen, obtained using high-quality micro-computed tomography with a voxel size under 20 μm (David et al. 2016). The process of adapting the geometry to make it suitable as input for the mathematical analysis is similar to the one described in our previous research (Arán-Tapia et al. 2023). A polyhedral mesh of 351,716 cells was selected for the fluid region, ensuring that the cell volume exceeds the otoconia volume to avoid numerical instabilities. A mesh independence analysis was performed to determine the optimal configuration (see Mesh analysis in Supplemental Digital Content 1, http://links.lww.com/EANDH/B346).

Definition of the EM

The EM considered for the numerical simulation is based on the original EM (Epley 1992). The only modification made to the original maneuver is that it concludes with the patient sitting at the bedside (Table 1). Instead of returning to the same initial position, the body is rotated 90° on the *Z* axis, looking toward the side of the unaffected canal (right side). This variation is typically applied to facilitate the transition of the patient to the sitting position during step 4 of the maneuver (Pérez-Vázquez et al. 2018). It is expected that this will not cause a significant effect on the otoconia path, as the *Z* axis of rotation is aligned with the direction of gravity. Also note that the initial position of otoconia is assumed to be at the bottom of the canal, where the force of gravity would eventually send them after an indeterminate amount of time when the head of the patient is completely upright, as in the natural position (Fig. 1B).

To investigate potential causes of treatment failure, several modifications were made in the substeps that were identified as challenging during the execution in clinical procedures. For that purpose, we introduced variations of 5° on the specific substep under study (Table 2). For step 4, we used a different perspective, now we consider that otoconia started at three different locations. In addition, a variation that combines steps 4 and 5 was implemented, named step 4-5. This modification was considered because the original EM indicated that these two steps should be performed separately (Epley 1992), but currently, these two steps are often performed together (without resting time between them).

Our definition of treatment failure is when otoconia do not achieve the frontside region of the utricle at the end of the complete maneuver, where the utricular macula is located (Fig. 5A). Considering this region as a low probability of treatment failure, other regions such as the common crux or the backside of the utricle were considered as a medium PFT. When the otoconia reached the semicircular canals, including the posterior ampulla, it was considered as a high probability of treatment failure. This criterion was also used for the numerical assessment of the maneuver steps.

Coordinate Systems for Rotation

The rotations in our model can be centered at either the head or the hip center, resulting in a more accurate representation of forces during the maneuver. The distance between the head and hip origins is typically 75 cm, based on anthropometry and the average human height (Roser et al. 2013). When rotating relative to the hip origin, the head coordinate system adjusts to ensure the head origin is always located in the center of the head. It is important to highlight that the orientations of the head and the hip coordinate system remain consistently aligned, as depicted in Figure 1A. As a result, the rotational planes presented in Tables 1 and 2 always follow the same coordinate system criterion.

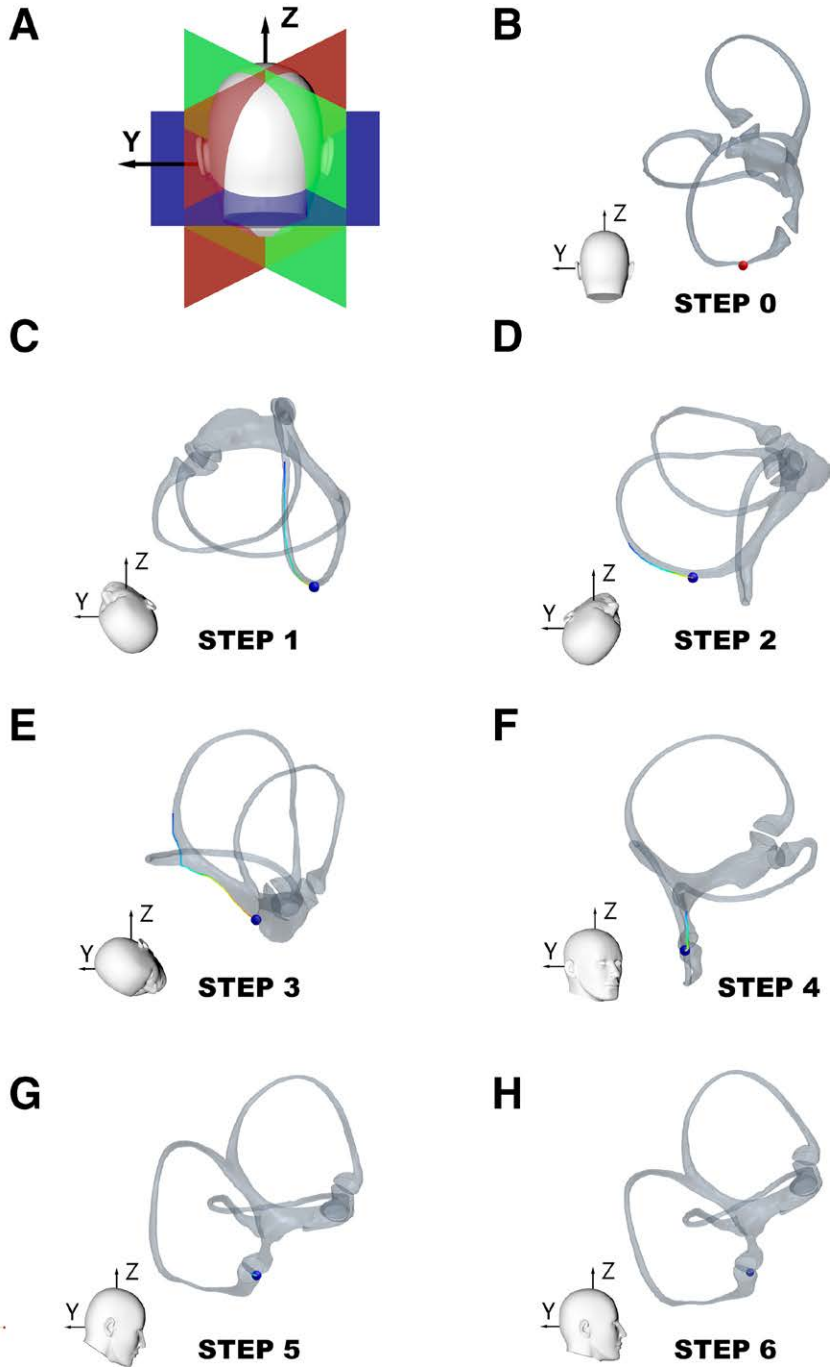

Fig. 1. Displacement of otoconia during the standard EM. A, Head position before maneuver starts. Also, idealized planes of the semicircular canals are shown, facilitating better visualization of the RHLH plane (blue), RALP plane (red), and LARP plane (green) orientations. B, Position of the membranous labyrinth before the EM starts. The red dot shows the initial position of otoconia. All the other images correspond to the different positions of the left membranous labyrinth and the head orientation for each step of the EM, along with the final position and paths of otoconia, for (C) step 1, (D) step 2, (E) step 3, (F) step 4, (G) step 5, and (H) step 6, and the end of the EM. EM indicates Epley maneuver; LARP, left anterior right posterior; RALP, right anterior left posterior; RHLH, right horizontal left horizontal.

A third coordinate system, called the posterior coordinate system, was created to calculate the position of each otoconia in relation to the center of the posterior semicircular canal. This coordinate system rotates with the geometry, consistently maintaining its position and axis orientations relative to the posterior semicircular canal. This approach enables us to compare numerical simulation results based on the angular position of the otoconia using polar coordinates.

Mathematical Model

The endolymphatic fluid is modeled as a laminar incompressible fluid with a dynamic viscosity of 8.15×10^{-4} Pa·sec (David et al. 2016). The boundary conditions for the fluid consist of no-slip wall condition and the geometry is closed without inlet or outlet walls. The membranous labyrinth walls enclosing the endolymphatic fluid are modeled as totally rigid walls because elasticity is not a significant factor at the frequencies typically

considered during EM (Breneman & Rabbitt 2009; Iversen & Rabbitt 2017; Rabbitt 2019). The cupula walls are also assumed to be rigid because the endolymphatic currents generated by cupula displacement are not strong enough to move otoconia due to the differences in density between otoconia (2700 kg/m^3) (Squires et al. 2004) and the endolymphatic fluid (1000 kg/m^3) (David et al. 2016).

The mathematical model used to simulate the behavior of the endolymphatic fluid was coupled with a spherical particle model to represent otoconia within the fluid. A total of 100 otoconia with varying sizes were simulated in the study, ranging from 3 to 30 μm in increments of 3 μm, which reflects the range observed in humans (Jang et al. 2006). This resulted in the creation of 10 different groups, each consisting of 10 particles. Bidirectional interactions were considered between the fluid and particles, as well as between the particles and walls, but collisions between particles were not simulated to reduce computational costs. This assumption was made due to the small volume of the particles compared with the fluidic volume, which suggests minimal interaction between particles during their movement (Boselli et al. 2014). To improve the stability and accuracy of the solution, a time-step of 0.001 sec was used (as detailed in Mesh Analysis in Supplemental Digital Content 1, http://links.lww.com/EANDH/B346).

The Reynolds numbers that describe the ratio of viscous forces to inertial forces in the endolymph are typically very small (Brody et al. 1996). Therefore, the model does not consider turbulence terms, and the inertial forces associated with fluid motion are negligible compared with the viscous forces affecting otoconia motion (Hain et al. 2005). In addition, the Womersley number, which characterizes the relationship between the frequency of a pulsating flow and the viscous effects, is low because the typical rotation function during the EM falls within the operating range of frequencies for the semicircular canals (Obrist 2019). This allows for an endolymphatic Poiseuille flow inside the semicircular canals. Lastly, considering otoconia as particles immersed in the endolymphatic fluid, the Froude number, which relates the inertial forces to the gravity forces, determines that both inertial and gravity forces are equally important during rotation. The Stokes number, which describes the relationship between the time scales for slow particle motion and the cupula model, is smaller for larger otoconia and larger for smaller ones, resulting in different properties (Obrist & Hegemann 2008) (see Dimensionless numbers for further details in Supplemental Digital Content 1, http://links.lww.com/EANDH/B346).

The solution for the endolymphatic flow is obtained by solving the Navier–Stokes equations, incorporating the inertial terms resulting from the rotation of the head, such as Coriolis (f_{co}), centrifugal (f_c), and Euler (f_e) forces, as well as the drag force exerted by otoconia (f_d),

$$\rho_e \frac{\partial v}{\partial t} + \rho_e(v \cdot \nabla v) = -\nabla p + \mu_e \nabla^2 v + f_{co} + f_c + f_e + f_d \quad (1)$$

where v is the endolymphatic fluid velocity vector relative to the velocity of the rotating reference frame, p is the pressure, and ρ_e is the density of the endolymph.

TABLE 1. Steps and substeps of the standard EM considered for the numerical simulations

Step	Substep	Plane of Rotation	Origin	Rotation (°)
1	A	(0.000, 0.000, 1.000)	Head	45
1	B	(0.000, 1.000, 0.000)	Hip	–90
1	C	(0.000, 1.000, 0.000)	Head	–30
2	A	(0.866, 0.000, 0.500)	Head	90
3	A	(1.000, 0.000, 0.000)	Hip	90
4	A	(0.000, 1.000, 0.000)	Hip	90
4	B	(1.000, 0.000, 0.000)	Head	30
5	A	(0.000, 0.000, 1.000)	Head	45
5	B	(1.000, 0.000, 0.000)	Head	20
6	A	(1.000, 0.000, 0.000)	Head	–20

Positive displacement indicates an anticlockwise rotation, while negative denotes a clockwise rotation. The planes of rotation are defined based on the directions of the static coordinate system, but the origin of rotation varies depending on the substep being studied. For a clearer visualization of the head and membranous labyrinth orientation, please refer to the animation provided in Supplemental Digital Content 3 and Figure 1.
EM, Epley maneuver.

TABLE 2. Variations in the rotation angles considered to assess the effectiveness of the EM

Step	Substep	Plane of Rotation	Origin	Variation (°)
1	A	(0.000, 0.000, 1.000)	Head	30 < 45 < 60
1	C	(0.000, 1.000, 0.000)	Head	–15 < –30 < –45
2	A	(0.866, 0.000, 0.500)	Head	75 < 90 < 105
3	A	(1.000, 0.000, 0.000)	Hip	75 < 90 < 105
4		Initial position in the superior semicircular canal		
4		Initial position in the backside of the utricle		
4		Initial position in the frontside of the utricle		
4-5		No resting time between steps		
4-5	B	(1.000, 0.000, 0.000)	Head	0 < 20 < 90

For a more comprehensive view of these variations, refer to the head orientations depicted in Figure 3.
EM, Epley maneuver.

The displacement of the otoconium inside of the canal will be determined by the same forces as in Equation 1, together with the buoyancy (f_b) and gravitational (f_g) forces acting on the otoconium,

$$m_p(a_p + C\omega) = f_{co} + f_c + f_e + f_d + f_b + f_g \quad (2)$$

where m_p is the mass of the otoconium, a_p is the acceleration of the otoconium, C is the distance to the origin of rotation (depending on the substep can be head or hip origin), and ω is the angular velocity vector of the rotating reference frame based on the function given by Obrist (Obrist et al. 2010) and adjusted to the different conditions for each step (Tables 1 and 2).

Upon the completion of the rotational movement ($\omega = 0$ rad), all the inertial forces stop acting and only the drag force (generated by otoconia) acts over the endolymph, causing a displacement of the cupula that evokes the positional nystagmus (Equation 1). Hence, only the combined effect of the drag, buoyancy, and gravitational forces (Equation 2) will contribute to the transport of otoconia.

Despite the curved geometry of the semicircular canals, the settling time (the time necessary for the otoconium to achieve the final position) can be estimated using the Stokes formulae (Squires et al. 2004),

$$t = t_0 + ad^{-2} \quad (3)$$

indicating that larger otoconia settle faster than smaller ones, inversely proportional to the square of the diameter d . The parameter a depends on the viscosity of the endolymph and the difference between endolymph and otoconia densities. The initial time t_0 depends on the specific step of the maneuver under consideration.

The optimal rotation for each step will be the one that displaces the otoconia at the largest angle, as we have assumed an indefinite resting time to determine when all otoconia reach their final position. It is important to note that our definition of resting time does not include the time taken during the rotation (3 sec for each substep), and that there are no resting times between substeps within a given step.

RESULTS

Standard EM

Figure 1 presents the trajectory traced by otoconia during the standard EM. The first three steps are sufficient to displace the otoconia out of the posterior semicircular canal, as demonstrated in Figures 1C–E. The otoconia move 125.5°, 51.2°, and 34.6°, respectively, resulting in a total displacement of 211.3° as required to exit the semicircular canal region and enter the common crux. Approximately 82% of this displacement occurs when the membranous labyrinth model is at rest, with the remaining 18% happens during the rotation. After completing step 3 (Fig. 1E), the otoconia are positioned at the backside of the utricle. During step 4 (Fig. 1F), all otoconia, regardless of its size, move into the posterior ampullar region from the utricular side. Successive steps 5 and 6 (Figs. 1G, H) cannot solve this situation and otoconia remain in the posterior ampulla at the end of the maneuver. According to the criteria outlined in the definition of the maneuver, the standard EM cannot be considered successful as otoconia do not finish in the frontside of the utricle, where the utricular macula is located.

Despite the path followed by the otoconia was approximately similar regardless of its diameter, the time needed to reach the same final position varies depending on their diameter (Fig. 2A). The resting times for steps 5 and 6 are not displayed because the otoconia are already trapped within the posterior ampulla (for further information, refer to Appendix A1 in Supplemental Digital Content 2, http://links.lww.com/EANDH/B347). Figure 2B illustrates the resting time required for the otoconia to exit the posterior semicircular canal (refer to the animation provided in Supplemental Digital Content 4 for the case of 30 µm otoconia studied). The resting time corresponding to step 3 is the time required for otoconia to exit the posterior semicircular canal and enter the common crux (see Appendix A2 in Supplemental Digital Content 2, http://links.lww.com/EANDH/B347).

Numerical Assessment of Each Step in the EM

The previous section provided a description of the standard EM and its effects on the vestibular labyrinth of the human

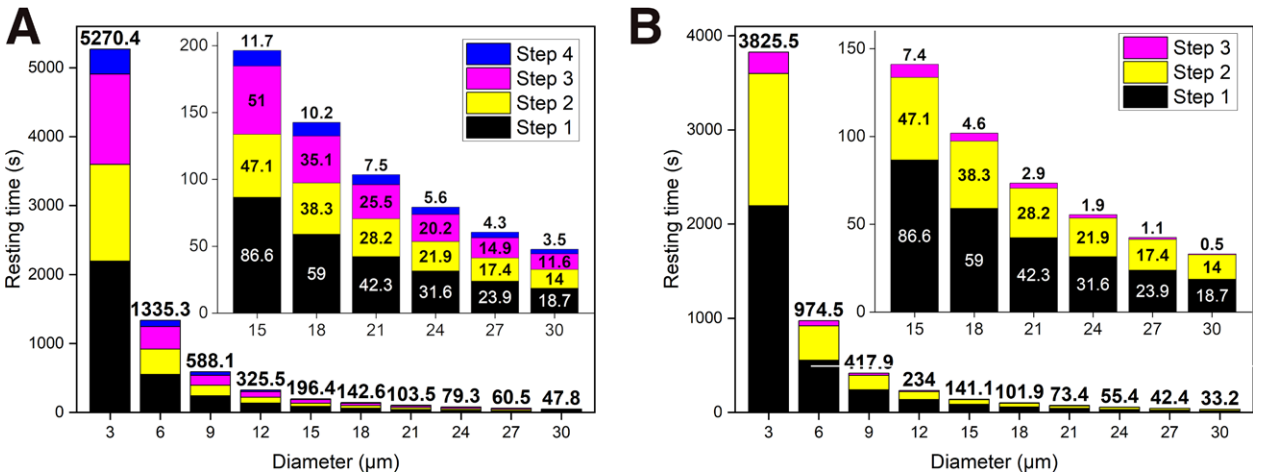

Fig. 2. Resting times required for otoconia to reach final position at each step for each otoconium diameter. A, Resting times are recorded for all the steps before otoconia falls back to the other side of the ampulla (the inset provides a zoom for larger otoconia diameters). B, Resting times recorded until otoconia leaves the posterior semicircular canal (the inset provides a zoom for larger otoconia diameters). For additional information, refer to Appendix A in Supplemental Digital Content 2, http://links.lww.com/EANDH/B347, and the Supplemental Digital Content 4.

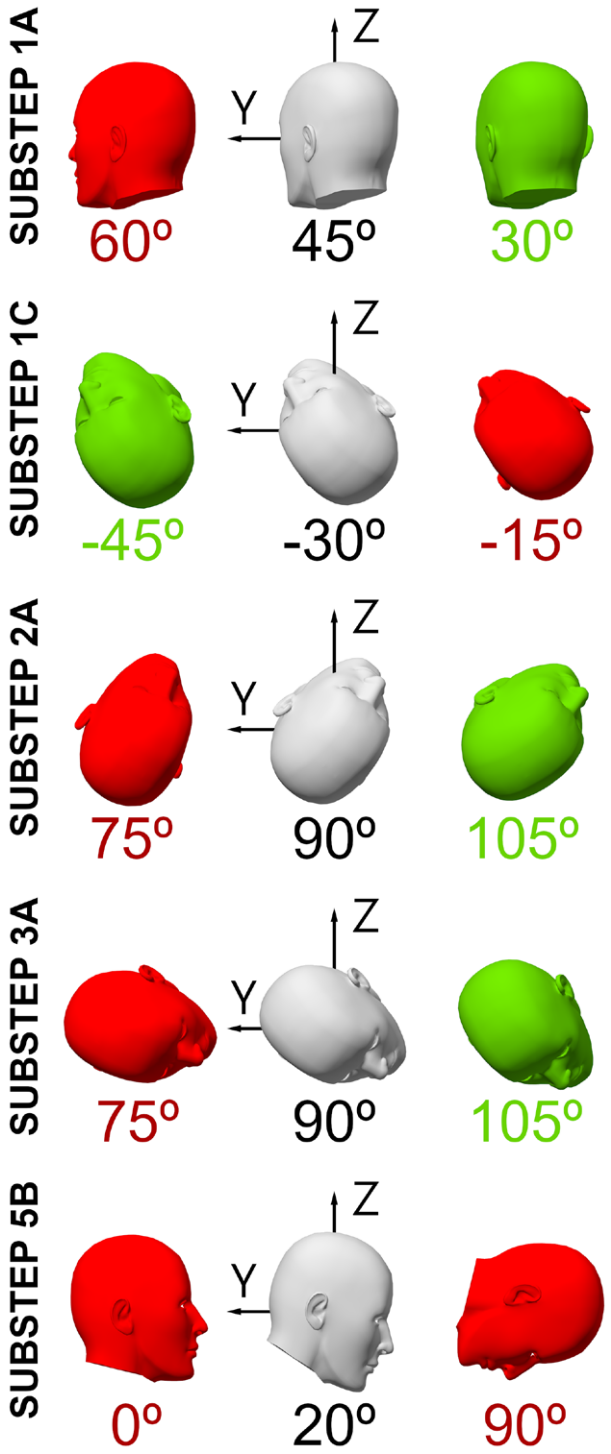

Fig. 3. Head orientations representing the ranges of angle variation studied for each substep, as outlined in Table 2. The standard position is denoted by gray, while red indicates worse performance and green indicates better performance. For the optimal position for substep 5B, refer to Figure 5.

specimen under consideration, highlighting potential causes of failure that may hinder the success of the procedure. In this section, we undertake an analysis of these causes, considering the modifications to the maneuver as presented in Table 2. A summary of the results for each substep is in Figure 3.

For the initial position of the EM, we studied different initial locations of the otoconia, and we found that even in the most unfavorable position, such as being close to the cupula, otoconia will advance along the semicircular canal during the next steps.

In the analysis of substep 1A (Appendix B1 in Supplemental Digital Content 2, http://links.lww.com/EANDH/B347), rotating an angle lower than the standard 45° provides a greater angular displacement for the otoconia. This displacement increases as we move away from the standard position. The resting time remains practically constant, indicating that otoconia can be displaced by a larger number of degrees without necessarily needing longer resting times. Conversely, angles larger than 45° yield a smaller displacement.

For the analysis of substep 1C (Appendix B1 in Supplemental Digital Content 2, http://links.lww.com/EANDH/B347), the angular displacement of the otoconia increased when angles of rotation are above the standard 30°, and decreased when below 30°.

In the analysis of step 2 (Appendix B1 in Supplemental Digital Content 2, http://links.lww.com/EANDH/B347), a rotation angle over 90° leads to a larger angular displacement of the otoconia, while angles under 90° result in worse outcomes. This effect becomes more pronounced as the angle deviates further from 90°.

The analysis of step 3 (Appendix B1 in Supplemental Digital Content 2, http://links.lww.com/EANDH/B347) indicates that an angular rotation below 90° can cause otoconia to fall inside the superior semicircular canal, potentially transforming a simple posterior BPPV into a multi-canal BPPV (Fig. 4A). On the other hand, the standard position of 90° leaves the otoconia on the backside of the utricle (Fig. 4B), which may result in otoconia falling into the ampullar region during the next step, as occurred during the standard EM. Positions above 90° move otoconia to the frontside of the utricle, practically placing them over the macula (Fig. 4C). Despite this, all positions effectively displace otoconia out of the posterior semicircular canal, and the time required for otoconia to exit the canal is nearly identical. However, the resting times differ depending on whether otoconia pass through the common crux or enter the superior semicircular canal.

For step 4, three different initial positions were studied (Appendix B2 in Supplemental Digital Content 2, http://links.lww.com/EANDH/B347). All otoconia that start at the backside of the utricle or in the superior semicircular canal fall into the ampullar region from the utricular side. When they start at the frontside of the utricle, smaller otoconia fall into the ampullar region, but larger ones do not. For the analysis of the combined step 4 and 5, the majority of otoconia fall inside the posterior ampullar region or end up at the backside of the utricle, regardless of the initial position chosen for step 4 (Appendix B3 in Supplemental Digital Content 2, http://links.lww.com/EANDH/B347).

Last, for this combined step 4-5, the substep 5B has been analyzed. When otoconia start in the backside of the utricle, all of them fall into the ampullar region. This indicates that combining steps 4 and 5 produce similar results as implementing them separately.

When the starting position of the otoconia is in the frontside of the utricle, larger particles are displaced toward the backside

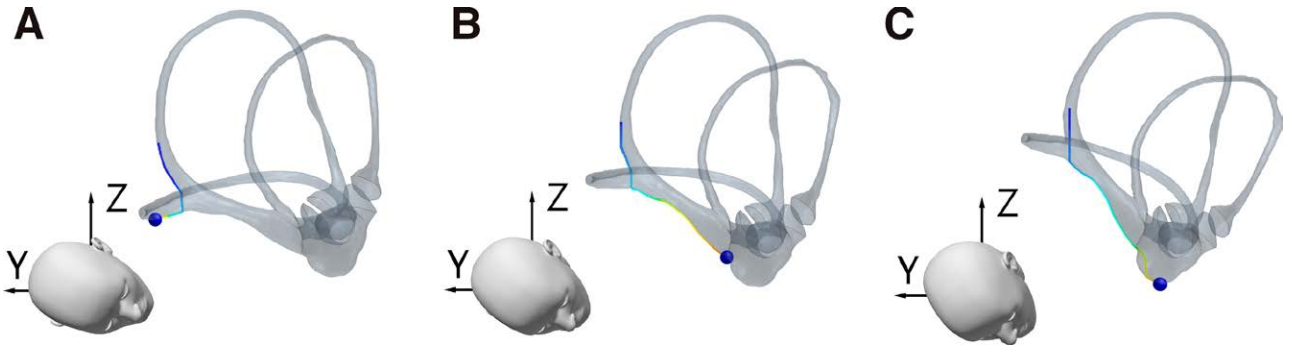

Fig. 4. Different positions reached by otoconia when it is applied the step 3 with a rotation angle of (A) 75°, (B) 90°, and (C) 105°.

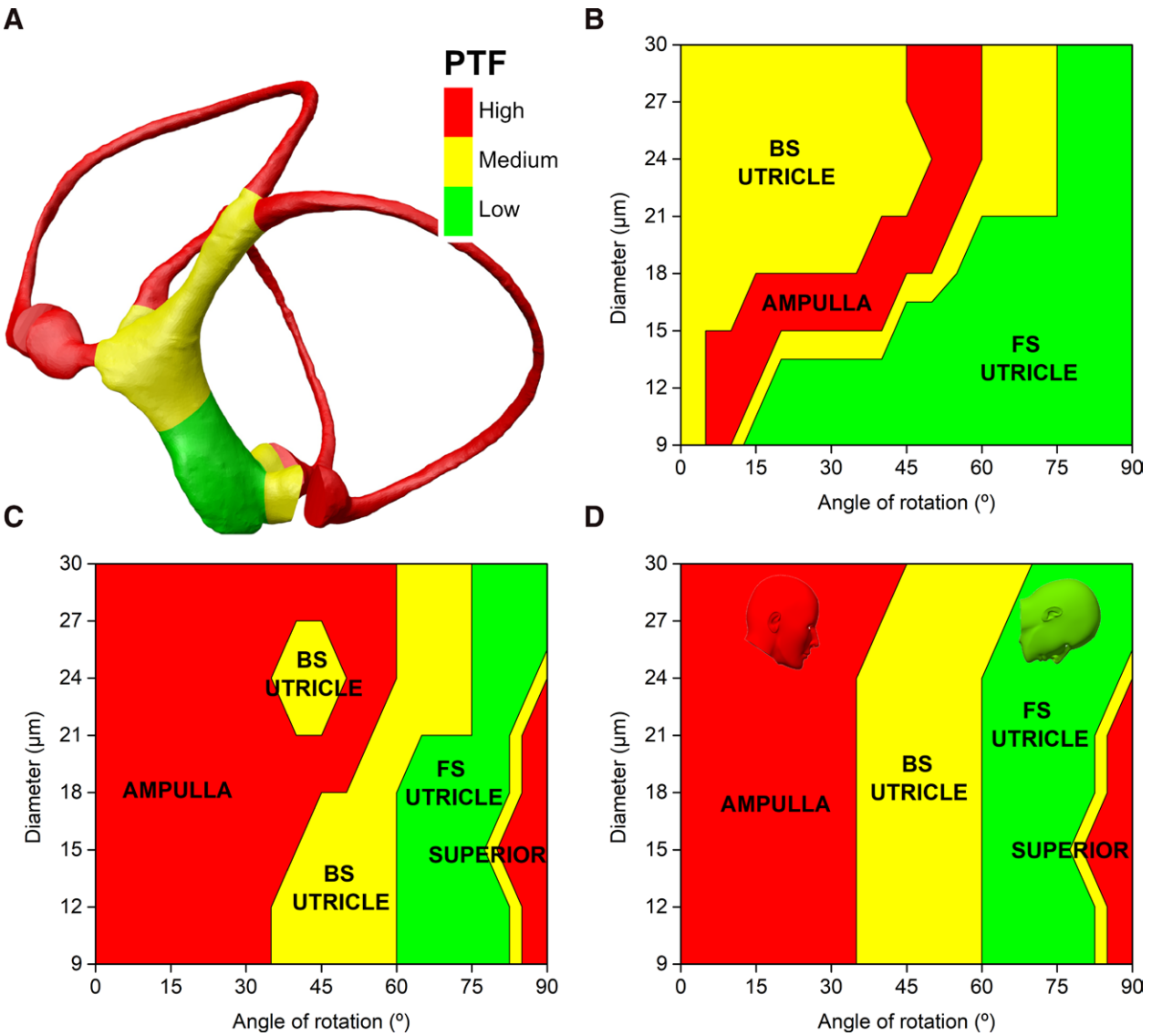

Fig. 5. Final position of otoconia depending on their diameter and the angle of nose-down rotation in the substep 5B. A, Regions of the membranous labyrinth classified by different PTF. The yellow region positioned between the frontside of the utricle (green), the posterior ampulla (red), and the common crux (yellow region that connect posterior and superior semicircular canals) can be identified as the backside of the utricle. For otoconia starting in (B) the frontside of the utricle, (C) the superior semicircular canal, and (D) the combination of both. A, The orientation of the membranous labyrinth corresponds to 75° nose-down, aligning with the green head orientation depicted in D. The standard 20° nose-down orientation is represented by the red head. A visual example of otoconia located in the backside of the utricle or the posterior ampulla can be seen in Figures 1E, F, respectively. As an instance of otoconia situated in the superior semicircular canal, reference can be made to Figure 3A. PTF indicates probabilities of treatment failure.

of the utricle or the posterior ampulla, while the smaller ones remain in the frontside of the utricle. Figure 5B shows a map of the final positions depending on the otoconium diameter and the angle of rotation for this scenario. Performing the standard 20° nose-down rotation causes some otoconia to fall in the ampullar region. However, if no rotation is applied in substep 5B, all otoconia remain in the backside of the utricle, which is not desirable. A large angle of rotation (larger than 75°) is needed to maintain all otoconia on the frontside of the utricle, leading to a successful outcome.

When the otoconia start in the superior semicircular canal, most of them move toward the common crux after substep 5A, with only the smaller ones remaining in the canal. If the standard 20° nose-down movement or no rotation during substep 5B is performed, all otoconia still fall inside the posterior ampulla. However, larger rotations (around 75°) force otoconia to move toward to the frontside of the utricle. In this case, angular displacements exceeding 80° might cause maneuver failure, as the smaller particles are unable to leave the superior semicircular canal. Figure 5C provides an equivalent map as presented in Figure 5B, but for this scenario.

Combining these results, a nose-down movement ranging between 75° and 80° during substep 5B ensures a successful step 4-5, independently of the initial position of the otoconia (Fig. 5D shows a combined map for scenarios shown in Figs. 5B, C).

DISCUSSION

Physics Behind the EM

The movement of the otoconia inside the semicircular canals in our model is consistent with previous results based on one-dimensional, two-dimensional, and three-dimensional models (Rajguru et al. 2004; Squires et al. 2004; Obrist & Hegemann 2008) or particle models using the Lattice–Boltzmann method (Djukic & Filipovic 2017). Our study focuses on applying theoretical knowledge regarding the forces affecting BPPV, to facilitate the understanding of otoconia displacements during the EM. This could provide helpful insights and answers for clinicians, potentially leading to an improved success rate of the EM.

During the rotation, otoconia transport is primarily determined by the inertial forces. These forces become more significant for rotations with respect to the hip center due to the larger distance from the origin of rotation. In fact, when rotations with respect to the head center are applied, the inertial forces decrease and become approximately equal to gravitational forces. Therefore, all forces presented in Equation 2 are relevant (see Dimensionless numbers in Supplemental Digital Content 1, http://links.lww.com/EANDH/B346). In addition, faster rotations result in increased inertial forces because they are linearly proportional to the angular velocity. This strategy is also used in other CRP called the Semont maneuver, which relies on high angular velocity for its success (Faldon & Bronstein 2008; Bhandari et al. 2021). In contrast, our results for the EM indicate that the displacement of otoconia during the rotation is relatively small compared with their displacement after rotation. This observation aligns with the established understanding that the EM is a CRP based on gravitational forces rather than inertial forces (Epley 1992).

After the rotation, the movement of the otoconia is primarily determined by the forces presented in Equation 2, without the influence of inertial terms. Among these forces, the gravitational force is always dominant, causing otoconia to move along the direction of gravity. As a result, the otoconia can be observed rolling down along the walls of the labyrinth and detaching from them at specific points, which depend on the anatomical properties of the membranous labyrinth and its orientation with respect to the gravitational force (Fig. 1). As the size of the otoconium diminishes, the gravitational force dominance is reduced, making the buoyancy force more relevant. Because the buoyancy force always acts in the opposite direction to gravity, smaller otoconia move at a lower velocity compared with larger ones, and thus, require more time to reach their final position (Yu et al. 2018). This phenomenon also explains why otoconia move in a single-file along the bottom inside surface of the canal, as predicted theoretically and observed experimentally in animals with glass microbeads inserted in their canals (Rajguru & Rabbitt 2007; Boselli et al. 2014). Our resting time analysis agrees with this description, showing that resting time increases approximately in proportion to the square of the diameter (Fig. 2). This behavior closely aligns with the Stokes formula (Equation 3) and other studies that have compared it with the onset latency (Rajguru et al. 2004).

Incorporating a more complex model, such as one with elastic walls or sticky properties for otoconia due to the presence of remains of the otolithic membrane attached to them (Kao et al. 2017), or accounting for their collision, would likely increase the resting times. The resting times also could differ if accumulative otoconia were considered in certain portions of the geometry, as in canalith jam (Castellucci et al. 2019). However, this is not expected to occur in our model because the number of particles selected for the study is low and clumps of otoconia typically disperse during their motion along the semicircular canal (Boselli et al. 2014). Last, also note that these resting times were obtained with idealized spherical otoconia. When the shape factor is considered, otoconia with less spherical shapes (closer to the actual geometry of the otoconium) require longer resting times to achieve a successful EM (Yu et al. 2021).

Numerical Analysis

The initial position of the otoconia at the beginning of the EM depends on the canal geometry of each patient as the otoconia are positioned at minimum-potential-energy locations when the head is at rest. All the initial positions we studied for this human membranous labyrinth resulted in positive outcomes because the otoconia can advance along the semicircular canal during subsequent steps. This is due to the inertial force generated by the rotation, which helps expel otoconia away from the ampulla, preventing them from becoming trapped after the first step of the EM is executed.

Furthermore, the initial position may vary if a Dix–Hallpike test is performed before the EM. Our numerical simulations indicate that performing a Dix–Hallpike test before the EM would not significantly affect the outcome of the maneuver, and a lower nystagmus intensity during the EM may not necessarily indicate better or worse performance but simply that otoconia may have started with the advantage of being displaced away from the ampulla (which could explain fatigue [Boselli et al. 2014]). For instance, a clinical study observed an increase in the duration of nystagmus and the severity of symptoms during the loaded Dix–Hallpike test (Andera et al. 2020). On the basis of our analysis, rotating the head downward before initiating the

maneuver moves the otoconia closer to the ampullar region and results in a longer path during step 1. Despite these findings, it may be beneficial to maintain the head in the position shown in Figure 1B for several minutes to ensure that otoconia are in a resting position before initiating the maneuver.

There are no significant complications involved in the first and second steps of the EM, as all head positions studied are effective in achieving the displacement of the otoconia away from the ampullar region. The standard movements defined for these steps are based on an idealized orthogonal configuration of the semicircular canals. However, the orientation of the planes that create the canals can vary among individuals (Della Santina et al. 2005), suggesting that an optimal position dependent on this orientation can be expected. In this study, we did not conduct an extensive analysis comparing the behavior of otoconia concerning anatomical properties, such as the bent toroidal shape of the posterior semicircular canal or the range of angle variation concerning its normative plane. Despite this, we observed that, in certain instances, otoconia may descend freely, achieving larger velocities. In other instances, depending on the local orientation of the canal in relation to gravity, otoliths may roll along the wall, requiring more time to reach the same final position. Therefore, minimizing contact between otoconia and the wall allows them to travel larger distances without necessarily requiring longer resting times (Appendix B1 in Supplemental Digital Content 2, http://links.lww.com/EANDH/B347). On the basis of these observations, we suggest that the orientation and anatomical peculiarities of specific sections of the semicircular canal, where the otoconia are set to move, are more important than an averaged plane commonly used to determine angular relationships between the semicircular canals.

A discussion has arisen regarding the possibility to place the head of the patient on a pillow to alleviate anxiety (Lee et al. 2020), or moving the head less than 30° during step 1, particularly when the patient has limitations on their neck movement. Clinical studies have shown minor differences in effectiveness. However, our numerical analysis indicates that the greater the rotation angle below the bed plane for step 1, the larger the displacement of otoconia, potentially resulting in better effectiveness. This optimization with respect to the excursion angle was also observed in in vitro models for the Semont maneuver (Gebhart et al. 2021), where deviations larger than those studied here could result in errors during the equivalent step.

The displacement of the otoconia during step 2 is lower than that achieved during the previous step (Appendix B1 in Supplemental Digital Content 2, http://links.lww.com/EANDH/B347). This is because the local orientation of the posterior canal is less vertically oriented than in the first step, leading to irregularities and perturbations on the canal walls having a more significant impact. In this case, if the rotation of the head is much lower than the standard position, there is a possibility of otoconia falling toward the ampulla due to the change in slope of the posterior semicircular canal. To avoid this, it is also important to keep the position of the head below the bed plane during this step.

Step 3 is considered the most critical phase of the maneuver, and various modifications have been proposed to facilitate the entrance of the otoconia into the common crux (Rajguru et al. 2004). Our study reveals that even a minor deviation in the final position of the head can result in unsatisfactory outcomes. For instance, the downbeating nystagmus that occurs when the patient is returned to an upright head position (Oh et al. 2007) can be elucidated by the results presented in Figure 4. When the rotation angle is lower than 90° during the step 3, the otoconia may move inside the superior semicircular canal, potentially evoking a downbeating nystagmus in step 4. This observation was also reported in the vector analysis of BPPV (Aw et al. 2005). It is also worth noting that this step alone can position otoconia close to the macula if a rotation exceeding 90° is achieved. However, such rotations may be challenging, and the use of repositioning chairs could be beneficial in achieving this required positioning, especially in patients with limited mobility (Luryi et al. 2018).

Regardless of the initial position studied in step 4, the majority of otoconia fall into the posterior ampullar region. This confirms that when otoconia are at the backside of the utricle, there is a larger probability of them descending into the posterior ampulla, as observed in the standard EM (Fig. 1F). This occurs because the utricular floor is oriented along the horizontal plane, with the backside of the utricle positioned beneath the frontside.

Considering this, merging steps 4 and 5 into a single step, referred to as step 4-5, and concluding with an orientation of the membranous labyrinth that keeps otoconia far from the ampullar entrance is important for the success of the maneuver (Fig. 5D). Although there is controversy regarding the effectiveness of this last substep 5B, and it is typically discarded (Pérez-Vázquez et al. 2018; Mandalà et al. 2019), our numerical results indicate that not only it is essential but it is also the requirement for an angle of rotation larger than the 20°, which was originally proposed by Epley (Epley 1992). The reason behind this is that a larger angle of rotation allows otoconia to move along the utricular floor due to gravity in the direction of the frontside of the utricle, something that does not occur during the standard step (Fig. 1G). Furthermore, clinical studies have suggested that there are fewer residual symptoms when the head is inclined forward (Gan et al. 2021), which likely indicates that a greater number of otoconia have reached the frontside of the utricle, as suggested by our simulations.

Note that the otoconia finish in different locations despite starting at the same location during step 4-5 (Figs. 5B, C). This variation is due to the specific locations they reach during the rotation, as they experience slightly different inertial forces. Consequently, gravitational forces acting afterward displace them to different regions of the membranous labyrinth.

Last, the implementation of step 6, which involves placing the head of the patient in an upright position, results in the movement of otoconia to the posterior ampulla or the backside of the utricle. These findings imply that it is essential to maintain the previous position (75° nose-down at the substep 5B) for as long as possible, establishing a new stable position in the utricle, with the aim of placing otoconia over the utricular macula. Previous research conducted on bullfrogs has indicated that the expected time for otoconia re-fixation to the utricular macula ranges from 1 to 5 min (Otsuka et al. 2010). Furthermore, keeping otoconia in the utricle helps to their dissolution, as they are in contact with a larger volume of endolymphatic fluid (Zucca et al. 1998). Clinical trials have demonstrated that postural restrictions following the application of the EM lead to increased effectiveness (Hunt et al. 2012). Therefore, we suggest that postural restrictions utilized to prevent a vertical orientation of the utricle floor would impede the movement of otoconia into undesired regions and facilitate the re-fixation or dissolution of the otoconia.

TABLE 3. Summary of the EM, including the probability of treatment failure, potential errors, and possible solutions for each step

	PTF	Potential Error	Solution
Step 0	Low	Otoconia start close to the cupula wall.	Wait some minutes before starting the EM with the patient upright.
Step 1	Low	Otoconia experience delays.	In substep 1A rotate less than 45°. In substep 1C rotate more than 30°.
Step 2	Medium	Otoconia experience delays or move backward.	Rotate more than 90°. Maintain the head below the bed plane.
Step 3	High	Otoconia move into the superior semicircular canal or in the backside of the utricle.	Rotate more than 95° for otoconia to remain on the frontside of the utricle.
Step 4	High	Otoconia fall in the posterior ampulla.	Perform both step 4 and step 5, without resting time.
Step 4-5	High	Otoconia fall in the posterior ampulla.	Place the head in the step 5B around 75° to leave otoconia in the frontside of the utricle.
Step 6	Medium	Otoconia fall in the posterior ampulla or in the backside of the utricle.	Wait some minutes before starting step 6 to allow otoconia to re-fixate on the utricular macula.

EM, Epley maneuver; PTF, probability of treatment failure.

Clinical Overview

The use of numerical simulations of the EM might result in a very useful tool to enhance its success (Fig. 3). However, it is important to note that these findings were obtained for a specific human membranous labyrinth, and clinical validation of these results for a larger set of cases should be done. Nevertheless, we expect that some general recommendations can still be applied by clinicians to prevent potential failures during the EM (Table 3).

Steps 1 and 2 are useful for displacing the otoconia further away from the posterior ampulla and rotating more degrees than the standard position. Step 3 allows otoconia to exit the posterior semicircular canal, and slight deviations could move them into undesired regions. Steps 4 and 5 performed together are more effective than applying them independently. In addition, in substep 5B, rotating the head further down than the standard position could allow otoconia to reach the utricular macula, and maintaining this position for a few minutes would facilitate re-fixation.

The range of angular deviation studied (Table 2) falls within the range of errors observed during the EM with and without guidance devices (Moroz et al. 2021). In fact, a lack of precision was more frequently observed in steps of the maneuver where we found higher susceptibility of failure. Our findings suggest that success or failure may be determined by errors of only a few degrees, underscoring the importance of accurately positioning the head of the patient (a task that is not always accomplished). The use of Google Glass or rotary chairs is recommended, as they have been shown to enhance the precision of diagnosis and treatment for BPPV in clinical settings (Tan et al. 2014; West et al. 2019). These chairs can assist in aligning the membranous labyrinth at various angles as determined by numerical simulations, what could be potentially useful for personalized CRP.

Based on the physical description of the EM, the resting times obtained in this study should be considered as a minimum reference time needed for otoconia to achieve the final position during each step (see Appendix A in Supplemental Digital Content 2, http://links.lww.com/EANDH/B347). When comparing these resting times to those typically applied during the EM (Pérez-Vázquez et al. 2018; Mandalà et al. 2019), it becomes apparent that the 30 sec resting time currently used allows only the largest otoconia to leave the posterior semicircular canal (Fig. 2). Therefore, it is recommended that the EM be performed with resting times greater than 30 sec, which would likely reduce the unsteadiness or residual dizziness observed in some patients after the maneuver (Richard-Vitton & Viirre 2011; Martellucci et al. 2016). In fact, personalizing the EM by adapting the resting time of the maneuver depending on the size of the otoconium evoking the positional nystagmus for a certain patient would be the optimal approach. However, currently, it is not possible to determine with certainty the mixture of otoconia responsible for the nystagmus. Furthermore, the resting time required for the smallest otoconia size is on the order of tens of minutes for each step, while the time allotted for clinicians with each patient is usually limited to several minutes for the entire maneuver.

CONCLUSION

The results obtained from numerical simulations, using a micro computed tomography of a specific human membranous labyrinth, demonstrate that the standard EM is not uniformly effective and slight variations can significantly impact its success (Table 3). In addition, the resting times recommended to accomplish the maneuver are probably insufficient, because smaller otoconia require more time because of the smaller gravitational force they experience (Fig. 2). Through an individual analysis of each step of the EM, we identified potential causes of failure that may be related to the local singularities and orientation of the membranous labyrinth.

On the basis of our findings, we anticipate that a personalized approach, tailored to the specific anatomy of the membranous labyrinth of an individual patient, could be used in the future to improve the success rate of the EM, especially in patients that are refractory to the standard treatment. We emphasize that numerical simulations offer clinicians valuable insights that cannot be obtained from clinical or imaging observations.

ACKNOWLEDGMENTS

The simulations were run in the Supercomputer Center of Galicia (CESGA) and the authors acknowledge their support.

This research is supported by the Spanish Ministerio de Economía y Competitividad and European Regional Development Fund, research grant PID2022-138322OB-100 funded by MCIN/AEI/10.13039/501100011033 and by "ERDF A way of making Europe." Also, Xunta de Galicia funded this research under research grant no. 2021-PG036. This study is part of

a clinical trial funded by the Instituto de Salud Carlos III- (PI23/00248) and co-financed by the European Union (EU). This research was partially founded by the Universidade de Santiago de Compostela (Spain) under the program "Acelerador de Transferencia," 8 edition.

I.A.T. designed the models, performed the CFD simulations, analyzed the results, and wrote the original draft. All other authors (A.S.V., V.P.M., S.S.P., I.A., and A.P.M.) participated equally on supervision, conceptualization, and review of the manuscript.

This study utilized a human micro-CT from an open-source database (http://www.earbank.org/ariadne.php). Because no direct clinical study of patients was conducted, ethics approval or consent to participate was not required.

All data generated or analyzed during the present study have been incorporated into this published article and its supplementary information files. The original datasets used and analyzed during the present study are available from the corresponding author upon reasonable request.

The authors have no conflicts of interest to disclose.

Address for correspondence: Ismael Arán-Tapia and Alberto P. Muñuzuri, Universidade de Santiago de Compostela, Santiago de Compostela, Spain. E-mail: ismaelaran.tapia@usc.es; alberto.perez.munuzuri@usc.es

Received May 12, 2023; accepted January 23, 2024; published online ahead of print March 5, 2024

REFERENCES

Andera, L., Azeredo, W. J., Greene, J. S., Sun, H., Walter, J. (2020). Optimizing testing for BPPV—The loaded Dix-Hallpike. *J Int Adv Otol*, *16*, 171–175.

Arán-Tapia, I., Soto-Varela, A., Pérez-Muñuzuri, V., Santos-Pérez, S., Arán, I., Muñuzuri, A. P. (2023). Numerical simulations to determine the stimulation of the crista ampullaris during the Head Impulse Test. *Comput Biol Med*, *163*, 107225.

Aw, S. T., Todd, M. J., Aw, G. E., McGarvie, L. A., Halmagyi, G. M. (2005). Benign positional nystagmus: A study of its three-dimensional spatiotemporal characteristics. *Neurology*, *64*, 1897–1905.

Bhandari, A., Kingma, H., Bhandari, R. (2021). BPPV simulation: A powerful tool to understand and optimize the diagnostics and treatment of all possible variants of BPPV. *Front Neurol*, *12*, 632286.

Boselli, F., Kleiser, L., Bockisch, C. J., Hegemann, S. C. A., Obrist, D. (2014). Quantitative analysis of benign paroxysmal positional vertigo fatigue under canalithiasis conditions. *J Biomech*, *47*, 1853–1860.

Breneman, K. D., & Rabbitt, R. D. (2009). Piezo- and flexoelectric membrane materials underlie fast biological motors in the ear. *MRS Online Proc Library*, *1186*, 25–36.

Brody, J. P., Yager, P., Goldstein, R. E., Austin, R. H. (1996). Biotechnology at low Reynolds numbers. *Biophys J*, *71*, 3430–3441.

Castellucci, A., Malara, P., Brandolini, C., Del Vecchio, V., Giordano, D., Ghidini, A., Ferri, G. G., Pirodda, A. (2019). Isolated horizontal canal hypofunction differentiating a canalith jam from an acute peripheral vestibular loss. *Am J Otolaryngol*, *40*, 319–322.

Choi, S. J., Lee, J. B., Lim, H. J., Park, H. Y., Park, K., In, S. M., Oh, J. H., Choung, Y.-H. (2012). Clinical features of recurrent or persistent benign paroxysmal positional vertigo. *Otolaryngol Head Neck Surg*, *147*, 919–924.

David, R., Stoessel, A., Berthoz, A., Spoor, F., Bennequin, D. (2016). Assessing morphology and function of the semicircular duct system: Introducing new in-situ visualization and software toolbox. *Sci Rep*, *6*, 32772.

Della Santina, C. C., Potyagaylo, V., Migliaccio, A. A., Minor, L. B., Carey, J. P. (2005). Orientation of human semicircular canals measured by three-dimensional multiplanar CT reconstruction. *J Assoc Res Otolaryngol*, *6*, 191–206.

Djukic, T., & Filipovic, N. (2017). Numerical modeling of the cupular displacement and motion of otoconia particles in a semicircular canal. *Biomech Model Mechanobiol*, *16*, 1669–1680.

Epley, J. M. (1992). The canalith repositioning procedure: For treatment of benign paroxysmal positional vertigo. *Otolaryngol Head Neck Surg*, *107*, 399–404.

Faldon, M. E., & Bronstein, A. M. (2008). Head accelerations during particle repositioning manoeuvres. *Audiol Neurootol*, *13*, 345–356.

Gan, Z., Zhou, S., Yang, H., He, F., Wei, D., Bai, Y., Wang, Y., Wang, Y., Fu, W., Han, J. (2021). Self-treatment of posterior canal benign paroxysmal positional vertigo: A preliminary study. *Front Med (Lausanne)*, *8*, 654637.

Gebhart, I., Götting, C., Hool, S.-L., Morrison, M., Korda, A., Caversaccio, M., Obrist, D., Mantokoudis, G. (2021). Sémont maneuver for benign paroxysmal positional vertigo treatment: Moving in the correct plane matters. *Otol Neurotol*, *42*, e341–e347.

Grieser, B. J., Kleiser, L., Obrist, D. (2016). Identifying mechanisms behind the Tullio phenomenon: A computational study based on first principles. *J Assoc Res Otolaryngol*, *17*, 103–118.

Hain, T. C., Squires, T. M., Stone, H. A. (2005). Clinical implications of a mathematical model of benign paroxysmal positional vertigo. *Ann N Y Acad Sci*, *1039*, 384–394.

House, M. G., & Honrubia, V. (2003). Theoretical models for the mechanisms of benign paroxysmal positional vertigo. *Audiol Neurootol*, *8*, 91–99.

Hunt, W. T., Zimmermann, E. F., Hilton, M. P. (2012). Modifications of the Epley (canalith repositioning) manoeuvre for posterior canal benign paroxysmal positional vertigo (BPPV). *Cochrane Database Syst Rev*, *2012*, CD008675.

Iversen, M. M., & Rabbitt, R. D. (2017). Wave mechanics of the vestibular semicircular canals. *Biophys J*, *113*, 1133–1149.

Jang, Y. S., Hwang, C. H., Shin, J. Y., Bae, W. Y., Kim, L. S. (2006). Age-related changes on the morphology of the otoconia. *Laryngoscope*, *116*, 996–1001.

Johnson Chacko, L., Schmidbauer, D. T., Handschuh, S., Reka, A., Fritscher, K. D., Raudaschl, P., Saba, R., Handler, M., Schier, P. P., Baumgarten, D., Fischer, N., Pechriggl, E. J., Brenner, E., Hoermann, R., Glueckert, R., Schrott-Fischer, A. (2018). Analysis of vestibular labyrinthine geometry and variation in the human temporal bone. *Front Neurosci*, *12*, 107.

Kao, W. T. K., Parnes, L. S., Chole, R. A. (2017). Otoconia and otolithic membrane fragments within the posterior semicircular canal in benign paroxysmal positional vertigo. *Laryngoscope*, *127*, 709–714.

Lee, H. J., Jeon, E.-J., Lee, D.-H., Seo, J.-H. (2020). Therapeutic efficacy of the modified Epley maneuver with a pillow under the shoulders. *Clin Exp Otorhinolaryngol*, *13*, 376–380.

Lee, S.-H., & Kim, J. S. (2010). Benign paroxysmal positional vertigo. *J Clin Neurol*, *6*, 51–63.

Lopez-Escamez, J. A., Gamiz, M. J., Fernandez-Perez, A., Gomez-Fiñana, M. (2005). Long-term outcome and health-related quality of life in benign paroxysmal positional vertigo. *Eur Arch Otorhinolaryngol*, *262*, 507–511.

Luryi, A. L., Lawrence, J., LaRouere, M., Babu, S., Bojrab, D. I., Zappia, J., Sargent, E. W., Schutt, C. A. (2018). Treatment of patients with benign paroxysmal positional vertigo and severe immobility using the particle repositioning chair: A retrospective cohort study. *Ann Otol Rhinol Laryngol*, *127*, 390–394.

Mandalà, M., Salerni, L., Nuti, D. (2019). Benign positional paroxysmal vertigo treatment: A practical update. *Curr Treat Options Neurol*, *21*, 66.

Martellucci, S., Pagliuca, G., de Vincentiis, M., Greco, A., De Virgilio, A., Nobili Benedetti, F. M., Gallipoli, C., Rosato, C., Clemenzi, V., Gallo, A. (2016). Features of residual dizziness after canalith repositioning procedures for benign paroxysmal positional vertigo. *Otolaryngol Head Neck Surg*, *154*, 693–701.

Moroz, M., Choy, M., Lee, C. W., Hadfield, H., Lasenby, J., Stone, T., Bance, M. (2021). Evaluating the Epley canalolith repositioning procedure with and without a visual assistive device. *Otol Neurotol*, *42*, 765–773.

Obrist, D. (2019). Flow phenomena in the inner ear. *Annu Rev Fluid Mech*, *51*, 487–510.

Obrist, D., & Hegemann, S. (2008). Fluid-particle dynamics in canalithiasis. *J R Soc Interface*, *5*, 1215–1229.

Obrist, D., Hegemann, S., Kronenberg, D., Häuselmann, O., Rösgen, T. (2010). In vitro model of a semicircular canal: Design and validation of the model and its use for the study of canalithiasis. *J Biomech*, *43*, 1208–1214.

Oh, H. J., Kim, J. S., Han, B. I., Lim, J. G. (2007). Predicting a successful treatment in posterior canal benign paroxysmal positional vertigo. *Neurology*, *68*, 1219–1222.

Otsuka, K., Suzuki, M., Shimizu, S., Konomi, U., Inagaki, T., Iimura, Y., Hayashi, M., Ogawa, Y. (2010). Model experiments of otoconia stability

after canalith repositioning procedure of BPPV. *Acta Oto-Laryngologica*, *130*, 804–809.

Pérez-Vázquez, P., Franco-Gutiérrez, V., Soto-Varela, A., Amor-Dorado, J. C., Martín-Sanz, E., Oliva-Domínguez, M., Lopez-Escamez, J. A. (2018). Practice guidelines for the diagnosis and management of benign paroxysmal positional vertigo otoneurology committee of Spanish otorhinolaryngology and head and neck surgery consensus document. *Acta Otorrinolaringol Esp*, *69*, 345–366.

Rabbitt, R. D. (2019). Semicircular canal biomechanics in health and disease. *J Neurophysiol*, *121*, 732–755.

Rajguru, S. M., Ifediba, M. A., Rabbitt, R. D. (2004). Three-dimensional biomechanical model of benign paroxysmal positional vertigo. *Ann Biomed Eng*, *32*, 831–846.

Rajguru, S. M., Ifediba, M. A., Rabbitt, R. D. (2005). Biomechanics of horizontal canal benign paroxysmal positional vertigo. *J Vestib Res*, *15*, 203–214.

Rajguru, S. M., & Rabbitt, R. D. (2007). Afferent responses during experimentally induced semicircular canalithiasis. *J Neurophysiol*, *97*, 2355–2363.

Rey-Martinez, J., Altuna, X., Cheng, K., Burgess, A. M., Curthoys, I. S. (2020). Computing endolymph hydrodynamics during head impulse test on normal and hydropic vestibular labyrinth models. *Front Neurol*, *11*, 289.

Richard-Vitton, T., & Viirre, E. (2011). Unsteadiness and drunkenness sensations as a new sub-type of BPPV. *Rev Laryngol Otol Rhinol (Bord)*, *132*, 75–80.

Roser, M., Appel, C., Ritchie, H. (2013). *Human Height*. Our World in Data.

Senofsky, N., Faber, J., Bozovic, D. (2023). Vestibular drop attacks and Meniere's disease as results of otolithic membrane damage—A numerical model. *J Assoc Res Otolaryngol*, *24*, 107–115.

Squires, T. M., Weidman, M. S., Hain, T. C., Stone, H. A. (2004). A mathematical model for top-shelf vertigo: The role of sedimenting otoconia in BPPV. *J Biomech*, *37*, 1137–1146.

Tan, J., Yu, D., Feng, Y., Song, Q., You, J., Shi, H., Yin, S. (2014). Comparative study of the efficacy of the canalith repositioning procedure versus the vertigo treatment and rehabilitation chair. *Acta Otolaryngol*, *134*, 704–708.

van der Zaag-Loonen, H. J., van Leeuwen, R. B., Bruintjes, T. D., van Munster, B. C. (2015). Prevalence of unrecognized benign paroxysmal positional vertigo in older patients. *Eur Arch Otorhinolaryngol*, *272*, 1521–1524.

von Brevern, M., Radtke, A., Lezius, F., Feldmann, M., Ziese, T., Lempert, T., Neuhauser, H. (2007). Epidemiology of benign paroxysmal positional vertigo: A population based study. *J Neurol Neurosurg Psychiatry*, *78*, 710–715.

West, N., Bloch, S. L., Møller, M. N., Hansen, S., Klokker, M. (2019). Reposition chair treatment improves subjective outcomes in refractory benign paroxysmal positional vertigo. *J Int Adv Otol*, *15*, 146–150.

Wu, X., Yu, S., Shen, S., Liu, W. (2021). Quantitative analysis of the biomechanical response of semicircular canals and nystagmus under different head positions. *Hear Res*, *407*, 108282.

Yu, S., Wang, J., Guo, Y., Sun, X., Shen, S. (2018). A numerical investigation of the effects of benign paroxysmal positional vertigo on the balance function of the inner ear. *Comput Model Eng Sci*, *116*, 315–322.

Yu, S., Wang, J., Shen, S., Tang, Y., Sun, X., Liu, Y. (2021). Study of the biomechanical mechanisms of benign paroxysmal positional vertigo. *J Vestib Res*, *31*, 163–172.

Zucca, G., Valli, S., Valli, P., Perin, P., Mira, E. (1998). Why do benign paroxysmal positional vertigo episodes recover spontaneously? *J Vestib Res*, *8*, 325–329.